Journal of Applied Polymer Science

Production of polyvinylpyrrolidone/chiral diacid modified nanocrystalline Mg-substituted fluorapatite nanocomposites: Morphological and thermal characterization

Shadpour Mallakpour,[1,2,3] Marziyeh Khani,[1] Fereshteh Mallakpour,[4] Mohammadhossein Fathi[4]

[1]Department of Chemistry, Organic Polymer Chemistry Research Laboratory, Isfahan University of Technology, Isfahan 84156-83111, Islamic Republic of Iran

[2]Nanotechnology and Advanced Materials Institute, Isfahan University of Technology, Isfahan 84156-83111, Islamic Republic of Iran

[3]Department of Chemistry, Center of Excellence in Sensors and Green Chemistry, Isfahan University of Technology, Isfahan 84156-83111, Islamic Republic of Iran

[4]Department of Materials Engineering, Biomaterials Group, Isfahan University of Technology, Isfahan 8415683111, Islamic Republic of Iran

Correspondence to: S. Mallakour (E-mail: Mallak@cc.iut.ac.ir or Mallak777@yahoo.com or Mallakpour84@alumni.ufl.edu)

ABSTRACT: The main objective of this work was the production of novel polyvinylpyrrolidone/diacid modified Mg-substituted fluorapatite (DM-MFA) nanocomposites (NC)s, by sonication process. Mg-substituted fluorapatite (MFA) powders with a chemical composition of $Ca_{9.5}Mg_{0.5}(PO_4)_6F_2$ were prepared by mechanical alloying technique. Initially, surface of MFA was modified by bioactive chiral diacid monomer, *N*-trimellitylimido-L-leucine as a coupling agent to form DM-MFA nanoparticles. DM-MFA NPs were utilized as a filler, to give the NCs with potential bioactivity. Examination of transmission electron microscopy (TEM), and field emission scanning electron microscopy (FE-SEM) microphotographs displayed that, there is no aggregation of a large quantity of particles. The above NCs showed rather improved thermal stability compared with pure polymer. The improvement of thermal behavior was related to the uniform and good dispersion of DM-MFA in the polymer matrix as well as the strong hydrogen bonding between C═O of PVP and OH of DM-MFA. © 2016 Wiley Periodicals, Inc. J. Appl. Polym. Sci. **2016**, *133*, 44254.

KEYWORDS: bioactive diacid; Mg-substituted fluorapatite; polymer nanocomposites; polyvinylpyrrolidone; ultrasonic irradiation

Received 8 June 2016; accepted 31 July 2016
DOI: 10.1002/app.44254

INTRODUCTION

Within the last 15 years, the materials exhibiting geometric dimensions under 100 nm have gained increasingly attraction to the scientific world and motivated spirit of research on occasionally serious products for consumer as well as on fancy notions for future applications like molecular manufacturing or space elevators.[1–3] Nanocomposites (NC)s including polymeric and inorganic constituents have been attracting considerable attention as novel materials because they have new properties and numerous potential applications, defined by the nature of both macromolecules and inorganic parts.[4–8]

Hydroxyapatite [HA; $Ca_{10}(PO_4)_6(OH)_2$] is one of the most widely used bioceramics in the field of biomaterials, because it is a main inorganic constituent of the bone matrix. They are used chiefly as source of phosphorus for the fertilizer industry. Also, they have other applications for example cement, dental implant, ion exchange, catalysis, and chromatography.[9–12] HA contains calcium ions replaceable by magnesium, lead, strontium, sodium, or zinc ions, in addition to hydroxyl and phosphate groups which can be substituted by fluoride, chloride, and bicarbonate ions afford apatites with reduced calcium content.[13]

Recently, pure fluorapatite [FA; $Ca_{10}(PO_4)_6F_2$] and fluorine-substituted HA (FHA) has attracted much consideration since it is useful for betterment of poor properties of HA in biomedical applications. Actually, this replacement causes a rise in chemical and structural stability and a decrease in mineral solubility.[14–16]

Mg-substituted HA prepared by Landi *et al.* made the material more biological in respect of composition, crystallinity, and morphology.[10,17] Keeping above points in view, Mg-substituted FA biomaterials are expected to have improved biological and biocompatibility properties than pure FA.[18]

Bioceramics and their composites are possible group of materials for medical applications. Owing to the notable interest related to the particular properties of the calcium phosphate-based composites, current researches were concentrated generally on the preparation and characterization of HA- and FHA-based NCs with suitable properties.[19,20] Newly, substantial consideration has been focused on preparing NCs wherein nanoapatite crystals are dispersed in appropriate polymer matrix.[21–24]

Nevertheless, the bonding between the ceramic nanoparticle and the macromolecule matrix is a significant parameter to improve properties of the NCs. However, the utilization of carefully chosen coupling agents has been demonstrated as a dependable way to reinforce the interfacial bonding between the filler and the matrix. Organosilane, organotitanate, organophosphonates, isocyanates, or phosphonic acid based coupling agents have formerly been utilized for the same target.[21,25–27]

In numerous studies of the FA surface reactions, it has been introduced that the surface holds active sites containing phosphate groups (POH) and calcium hydroxide groups (CaOH).[28,29] Three possible types of calcium and phosphorus groups sites at the FA surface were suggested $\equiv$CaOH, $\equiv Ca(OH)_2^-$, $\equiv CaOH_2^+$ and $\equiv PO_x$, $\equiv PO_xH$, and $\equiv PO_xH_2$, where $x = 1$, 2, or 3 (surface charges omitted), respectively.[30,31] Thus, the modification of the apatite surface with various inorganic and organic materials is expected to give novel functions to this material.[32]

Amongst all the valuable polymeric materials, polyvinylpyrrolidone (PVP) has excellent colloidal and complexing properties.[33] PVP has attracted substantial attention because of its lubricity, hydrophilicity, antiadhesive properties, and excellent biocompatibility.[34,35] PVP is a water-based macromolecule, and it has been considered an ecofriendly, biocompatible, and nontoxic polymer.[36] The incorporation of inorganic nanoparticles into a macromolecule matrix can result in substantial enhancements in a variety of chemical and physical properties.[37] There are a few reports on the synthesis and characterization of PVP/HA composites.[38,39] Nevertheless Mg-substituted HA ceramics have been proposed for utilization in orthopedic and dental applications.[40] However, with the purpose of overcoming the disadvantage of synthesized apatite, a number of composites for example polymer or ceramic NCs have been used as repairing materials to improve biological applications.[38] Therefore, these NCs has this potential to be used for bone tissue engineering applications,[39,41] in the biomedical field, for example, in nonviral gene delivery[42] and in advanced medical and dental technologies; such NCs provide the facility to control biodegradability, bioactivity, and mechanical properties.

In our previous work, the surface of Mg-FHA NPs was modified by different bioactive amino acids to improve NPs dispersion in the polymer matrix.[43] To the best of our knowledge, there is no report on using chiral diacid based coupling agent in the preparation of bionanocomposite between MFA and PVP matrix. The present research effort contains in the development of novel potentially bioactive NCs via PVP as the matrix and chiral diacid modified Mg-substituted fluorapatite (DM-MFA) as the filler. *N*-trimellitylimido-L-leucine (TML) has been utilized as the coupling agent. The NCs were synthesized through a fast sonication method, which can possibly provide excellent dispersion of DM-MFA nanoparticles (NP)s in the PVP matrix yielding NCs with uniform nanostructure. We have also widely studied the morphology, dispersion, and thermal stability of the synthesized NCs.

EXPERIMENTAL

Materials

The PVP of average molecular weight 25,000 g mol^{-1} was obtained from Merck Chemical Co. It was utilized as received. The synthesis and biodegradable properties of chiral diacid monomer TML was reported by the previous investigates.[44,45]

Equipment

The Fourier transform infrared (FT-IR) spectra were documented via a Jasco-680 spectrophotometer (Japan) at wavenumber range of 400 to 4000 cm^{-1}. Thermal analysis of the samples was carried out using thermal gravimetric analysis (TGA) instrument (STA503 TA, Hüllhorst, Germany) under an atmosphere of nitrogen. The heat rate used for all samples under investigation is 20 °C/min. The X-ray diffraction (XRD) patterns were performed on dried powder samples and were obtained with a Philips X'PERT MPD (Netherlands) diffractometer operating at current of 40 mA. The Cu-Kα radiation source ($\lambda = 1.54056$ Å) was used in the range of 10 to 60° at a scanning rate of 0.03°/s. Field emission scanning electron microscopy (FE-SEM) was performed using HITACHI (S-4160) (Tokyo, Japan). Samples were coated with gold in vacuum to perform the FE-SEM experiment. To analyze the nanostructure samples, transmission electron microscopy (TEM) (CM 120, Philips) was done at a working voltage of 100 kV. The reaction was performed under ultrasound waves via MISONIX ultrasonic liquid processor (XL-2000 SERIES). Ultrasonic irradiation was done with the probe of the ultrasonic horn being absorbed straightly in the mixture solution system with a frequency of 2.25×10^4 Hz and 100 W powers. Atomic force microscopy (AFM) topographic imaging of typical sample was performed at room temperature (RT) and atmospheric pressure using Nano S1/1 (BRUKER, Germany).

Synthesis of MFA Powder

Mg-substituted nanostructured FA powders were synthesized with a chemical composition of $Ca_{9.5}Mg_{0.5}(PO_4)_6F_2$ by mechanical alloying method.[46]

Surface Modification of Nanocrystalline MFA with Biodegradable TML Coupling Agent

Surface modification of MFA with TML was carried out as follows. Certain amount (15 wt %) of TML was dissolved in methanol as a solvent at R.T. One gram of MFA particles dried at 120 °C for 24 h were added into the aforementioned solution and were stirred vigorously at RT for 24 h. Thereafter the dispersed solution was ultrasonicated for 1 h. The particles thus treated were filtered off, thoroughly washed with methanol for several times to eliminate unreacted TML, and finally dried in an air oven at 50 °C for 24 h (Scheme 1).

Preparation of PVP/DM-MFA (PMFA) Composite

At first, one stock solution was prepared: PVP (0.1 g) was dissolved in distilled water at RT. Then, appropriate amounts of DM-MFA powders were added into the PVP solution to obtain the preferred weight percentages of DM-MFA from 3 to 7 wt %. The PVP/DM-MFA mixture was stirred at RT for 1 h

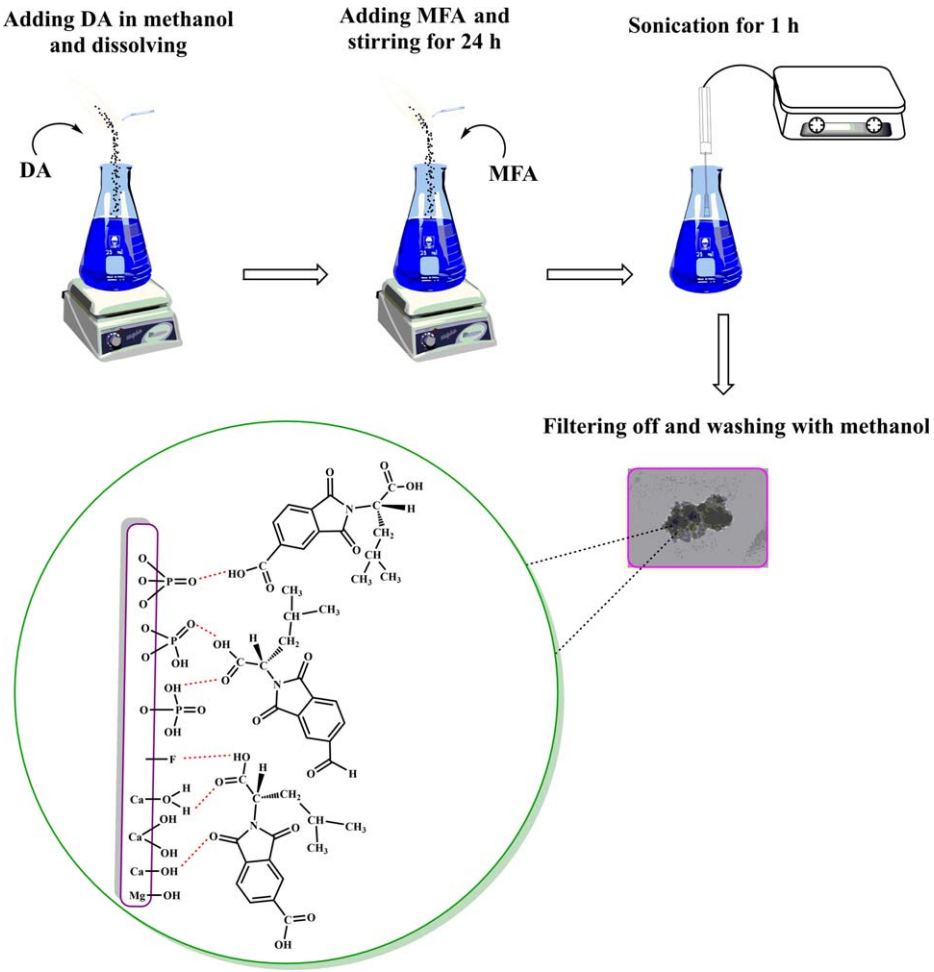

Scheme 1. Schematic representation of surface modification of MFA NPs with biodegradable TML. [Color figure can be viewed in the online issue, which is available at wileyonlinelibrary.com.]

and then ultrasonicated in a water bath for 30 min to improve the dispersion of DM-MFA NPs in polymer solution. After solvent evaporation, the samples were dried finally in an oven at 40 °C until reaching a constant weight. Scheme 2 shows a schematic model for the synthesis of the PMFA NCs structure.

RESULTS AND DISCUSSION

Infrared Study

Surface modification of FA with numerous compounds is one of the methods to reduce the surface energy and correspondingly to improve various properties and affinity to organic substances when utilized as a filler of cements and macromolecules. In this study, DM-MFA were constructed through modification of MFA with biodegradable diacid TML via an ultrasonic technique. To clarify the molecular interaction and binding between TML and MFA, FT-IR spectra were taken. The FT-IR spectra of the coupling agent TML (a),[44] pure MFA (b),[46] DM-MFA (c), PVP (d), and PMFA NC samples with different DM-MFA contents (e-g) are displayed in Figure 1. For TML [Figure 1(a)], the peaks at around 1782 to 1696 cm^{-1}, be owned by carbonyl stretching. Also, the peaks in the range 2916 to 2848 cm^{-1} are assigned to the stretching vibration of C—H bonds of biodegradable TML.[44] The characteristic peaks of PO_4^{3-}, which had four separate asymmetrical stretching vibration modes, namely, $\nu 1$ (963 cm^{-1}, P—O—P), $\nu 2$ (472 cm^{-1}, P—O), $\nu 3$ (1000–1100 cm^{-1}, P—O), and $\nu 4$ (577 and 603 cm^{-1}, O—P—O) appeared in the spectrum of MFA and DM-MFA [Figure 1(b,c)].[47–49] In addition, the bands in the range 1425 to 1459 cm^{-1} and 3100 to 3550 cm^{-1} are related to vibration of C—O stretching of CO_3^{2-} and —OH stretching of lattice H_2O) [Figure 1(b,c)].[46–48] For DM-MFA, the peak at around 1706 and 1772 and 2954 cm^{-1} is apportioned to the stretching vibration of hydrogen-bonded —C=O groups and C—H bonds of TML, respectively. These peaks could not be identified in the spectra of MFA. From these data, it can be realized that the biodegradable coupling agent TML has been absorbed on the surface of MFA through the hydrogen bonding. The presence of DM-MFA in the polymer matrix showed few changes in the FT-IR spectra [Figure 1(e–g)], apparently because of the low DM-MFA content. It is possible to observe in Figure 1(e–g) that the characteristic absorption bands of the DM-MFA and PVP were observed. Therefore, the functional groups of the achieved NCs were confirmed by the data of FT-IR spectra.

X-ray Diffraction Data

The XRD pattern of MFA (a)[46], DM-MFA (b), pure PVP (c), PMFA NC (3 wt %) (d), and PMFA NC (7 wt %) (d), is

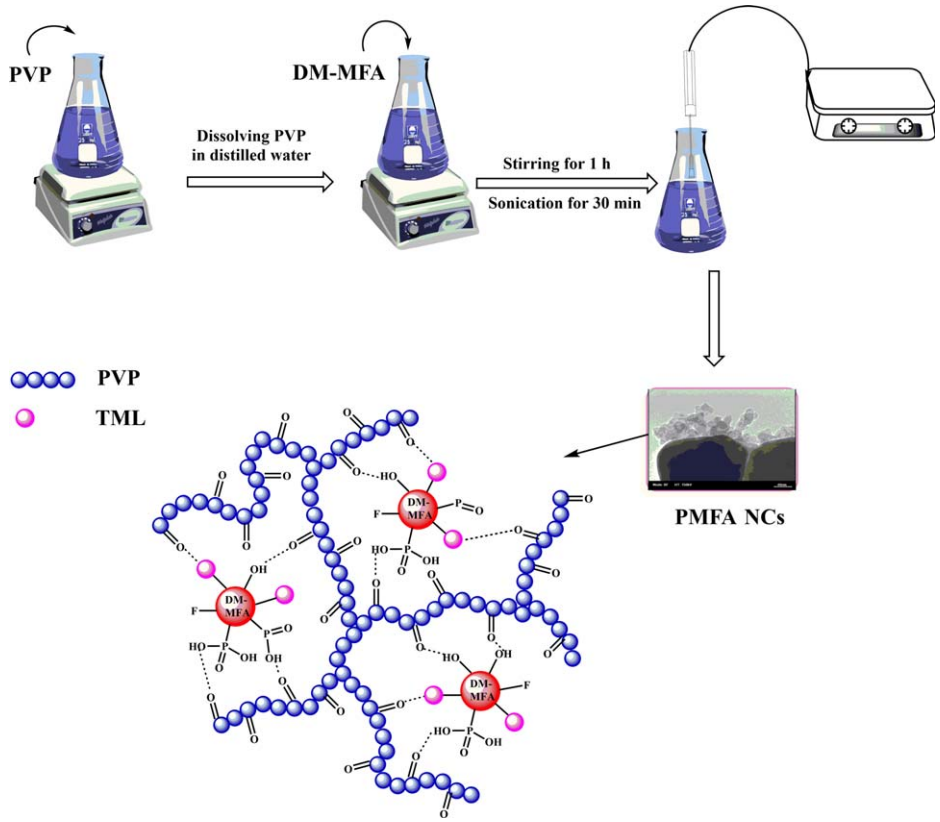

Scheme 2. Preparation process of PMFA NCs. [Color figure can be viewed in the online issue, which is available at wileyonlinelibrary.com.]

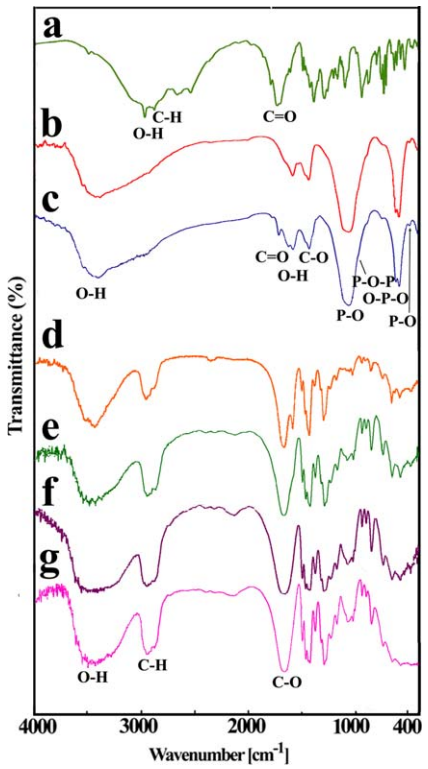

Figure 1. FT-IR spectra of TML (a), MFA (b), DM-MFA (c), PVP (d), and PMFA composites (e–g). [Color figure can be viewed in the online issue, which is available at wileyonlinelibrary.com.]

presented in Figure 2. Figure 2(a) showed the crystalline FA phase for pure MFA.[46] Predictably, the modification procedure has no effect on the crystalline phase of MFA since the diffraction peaks corresponding to the crystal planes remain

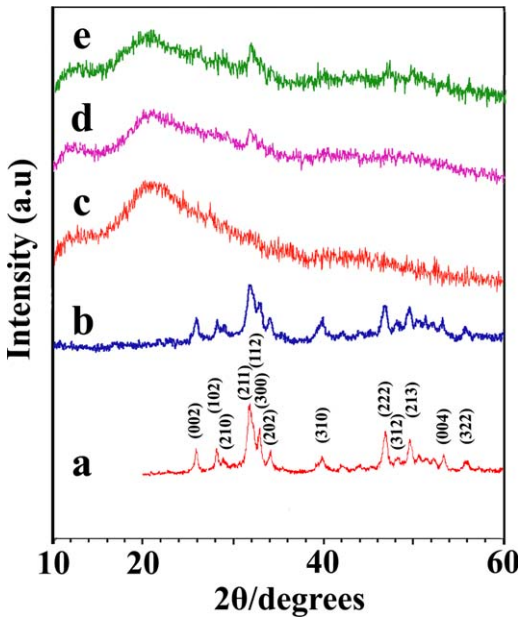

Figure 2. XRD curves of (a) MFA, (b) DM-MFA, (c) PVP, (d) PMFA (3 wt %), and (e) PMFA (7 wt %). [Color figure can be viewed in the online issue, which is available at wileyonlinelibrary.com.]

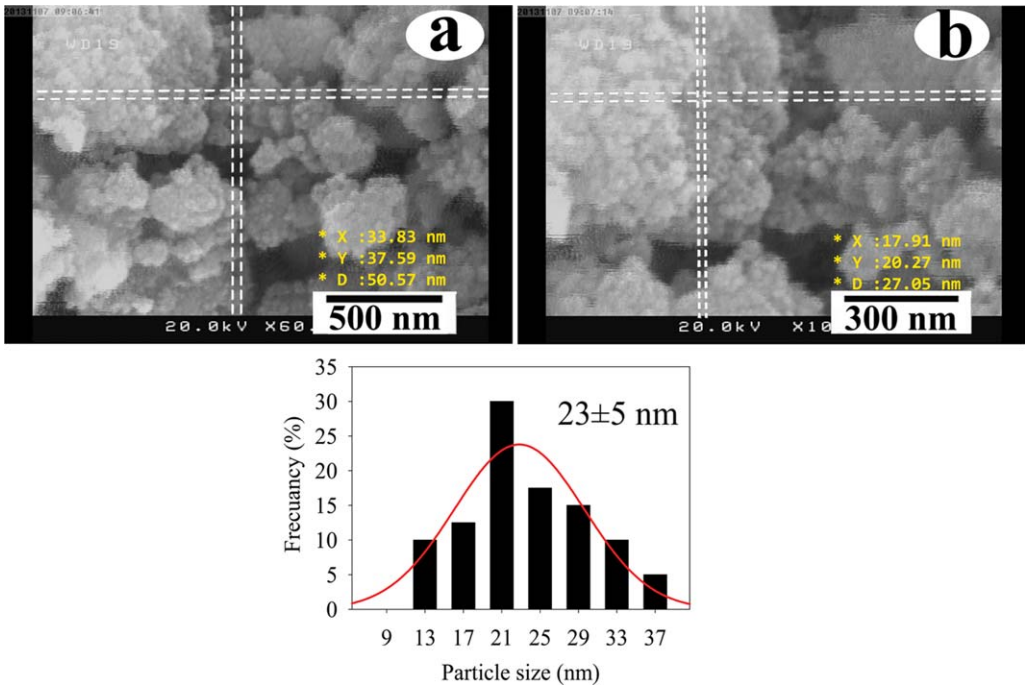

Figure 3. FE-SEM micrographs and particle size distributions of DM-MFA with different magnifications. [Color figure can be viewed in the online issue, which is available at wileyonlinelibrary.com.]

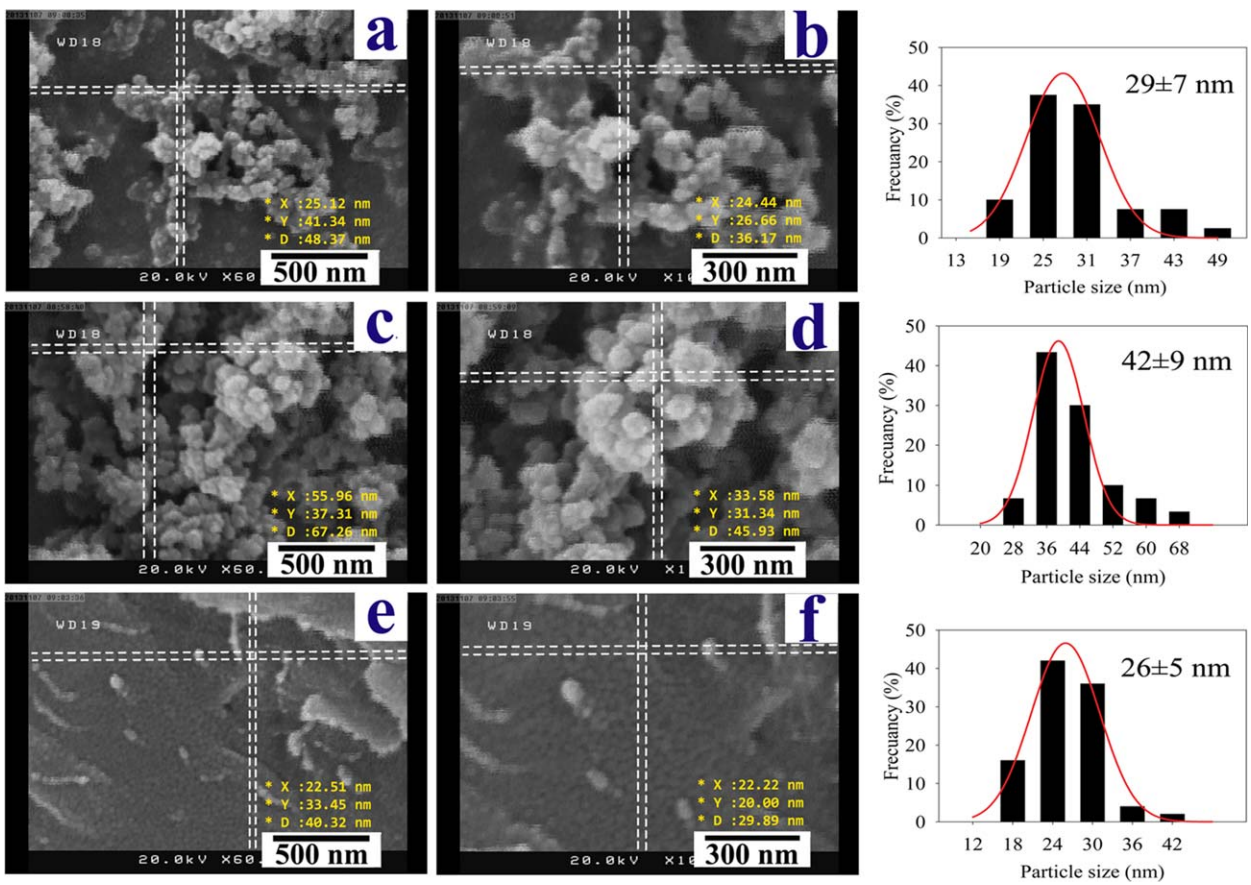

Figure 4. FE-SEM micrographs and particle size distributions of (a,b) PMFA (3 wt %), (c,d) PMFA (5 wt %), and (e,f) PMFA (7 wt %) with different magnifications. [Color figure can be viewed in the online issue, which is available at wileyonlinelibrary.com.]

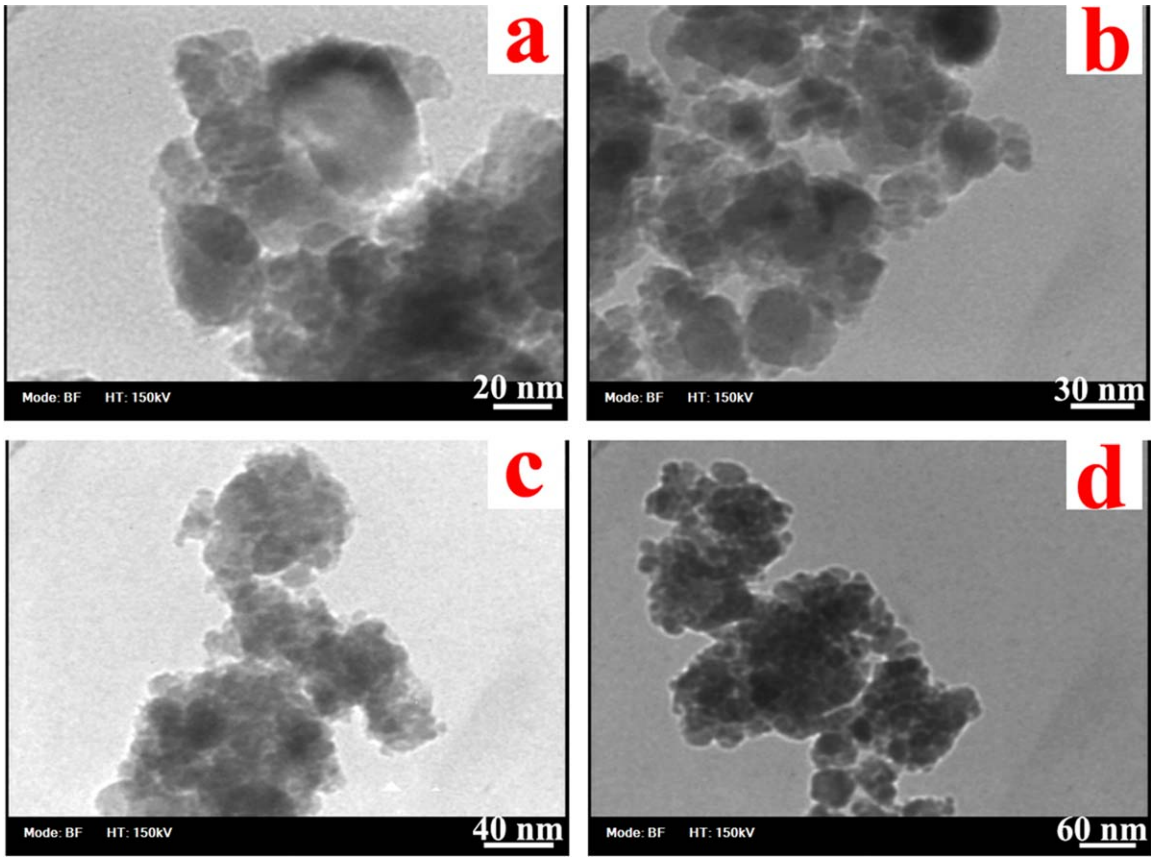

Figure 5. TEM micrographs of DM-MFA with different magnifications. [Color figure can be viewed in the online issue, which is available at wileyonlinelibrary.com.]

approximately equal for DM-MFA. The crystallite size of the MFA and DM-MFA powders was determined by XRD patterns and Williamson-Hall method [eq. (1)][50]

$$B \cos \theta = 0.9\lambda/D + \varepsilon \sin \theta \quad (1)$$

where B is the full-width at half maximum intensity, λ is the wave length of the X-ray utilized ($\lambda = 0.154056$ nm), D is the average crystallite size (nm), θ is the Bragg angle, and ε is the average strain. According to eq. (1), the crystallite size of the MFA is calculated to be 42 nm.[46] The crystallite size decreases to 28 nm for DM-MFA after modification. Also, the intensities of MFA peaks turned into weaker and wide in the presence of the TML. These data defined that ultrasonic irradiation reduces the crystallite size of DM-MFA due to the formation of many localized hot spots and a large number of seed nuclei in the solution through the ultrasound irradiation. The PVP is amorphous [Figure 2(c)] and displays a broad peaks around 11.5° and 22.5°.[51] From Figure 2(d,e), it can be seen that for the aforesaid NCs, most of the characteristic peaks at 2θ values of modified ceramic are kept entire. The shape and

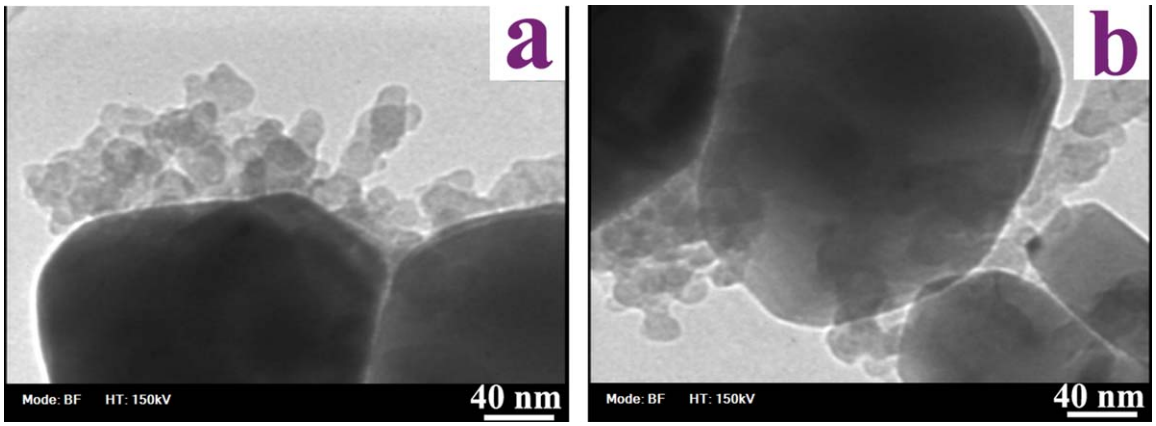

Figure 6. TEM micrographs of PMFA NC 5 wt %. [Color figure can be viewed in the online issue, which is available at wileyonlinelibrary.com.]

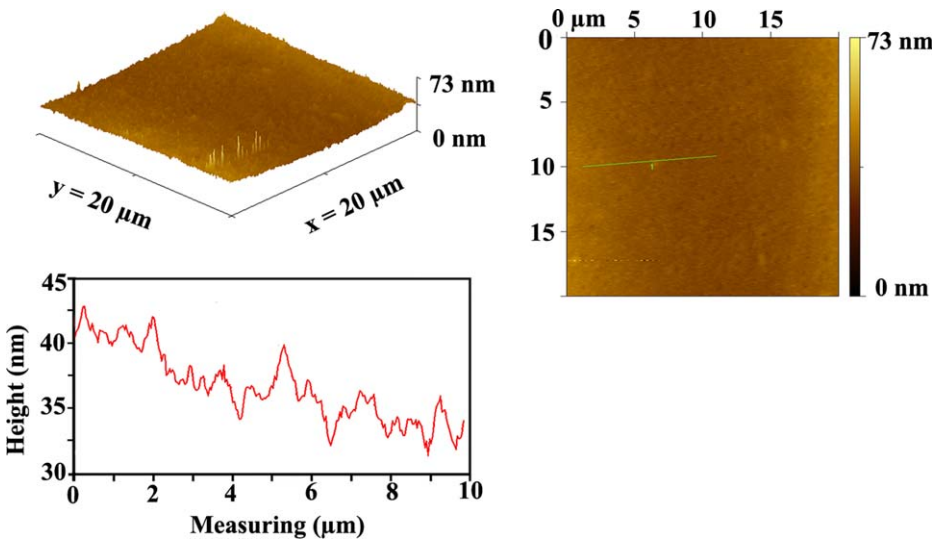

Figure 7. AFM scans and profile line of pure PVP. [Color figure can be viewed in the online issue, which is available at wileyonlinelibrary.com.]

position of PVP peaks has not altered. The increased weight percent ratio of DM-MFA has increased the intensity of the DM-MFA peaks in PMFA NCs.

Morphological Image Studies

FE-SEM images of obtained powders with different magnifications are displayed in Figures 3 and 4. The above-mentioned DM-MFA presented particles with irregular shape and temperately spherical (Figure 3). A number-frequency histogram is a characteristic method to exhibit the particle size and its distribution. From FE-SEM data it is clear that the mean particle size of DM-MFA is 23 ± 5 nm. Considering the Figure 4, it was found that PMFA NCs seem to have a rather homogenous distribution with size of about 26 to 42 nm.

So as to confirm the XRD results concerning the distribution of DM-MFA crystallites in the composite samples, TEM measurements were done. The TEM micrographs (Figures 5 and 6), shown the structural features of DM-MFA and the obtained NCs. The Figure 5 illustrates the crystals of DM-MFA with rather spherical shaped particles in nanometer range. Figure 6 represents the TEM micrograph of PMFA composite (5 wt %), in which the bright region represents the nanosized DM-MFA particles and the big area dark illustrate PVP matrix.

AFM Measurements

For observing the morphological changes at the surface, the AFM scans of the neat PVP and PMFA NC (5 wt %) are displayed in Figures 7 and 8, respectively. Before departing on a detailed interpretation of the AFM images of Figures 7 and 8, we should elucidate that, white domains in topography images refer to protruding sample locations (typically NPs).[52] For PMFA NC (5 wt %) (Figure 8), the surface is morphologically different from pure PVP. From the Figure 8, it is obvious that the DM-MFA NPs are dispersed homogeneously inside the polymer matrix which it can be seen from 2D and 3D images of PMFA. Thus, the PVP polymer stabilizes the filler from agglomeration by decreasing their mobility. The surface of PVP

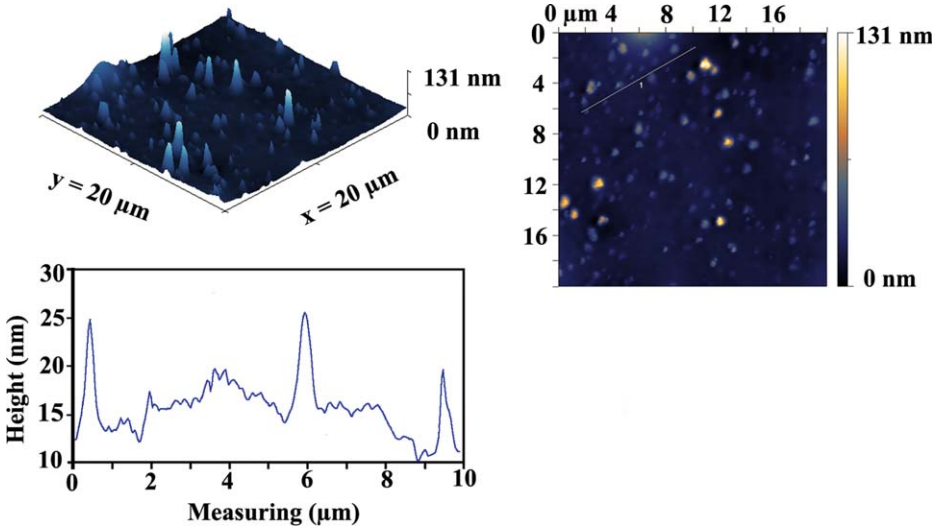

Figure 8. AFM scans and profile line of PMFA (5 wt %). [Color figure can be viewed in the online issue, which is available at wileyonlinelibrary.com.]

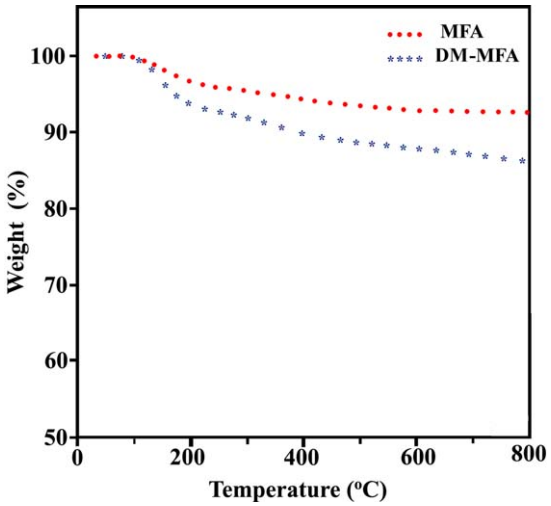

Figure 9. TGA thermograms of MFA, and DM-MFA under nitrogen atmosphere at heating rate of 20 °C/min. [Color figure can be viewed in the online issue, which is available at wileyonlinelibrary.com.]

matrix and the obtained NC were compared in terms of some roughness parameters, for example the average roughness (R_a) and the root mean square roughness (RMS).[53] R_a evaluates the deviation of a real surface from an ideal flat plane. As said by the AFM characterization, nanofillers change the surface morphology and roughness of the polymer. The R_a and RMS of the pure PVP is approximately 2.59 nm and 2.79 nm, respectively. Although it is increased for the PMFA NC (5 wt %) to 4.6 nm and 8.8 nm which indicates that the surface of PVP is covered with DM-MFA NPs and it could be ascribed to the good compatibility and physical interactions between DM-MFA NPs and the PVP matrix. This case could be attributed to existence of several OH functional groups on the surface of DM-MFA, which cause to form strong hydrogen bonding with PVP matrix.

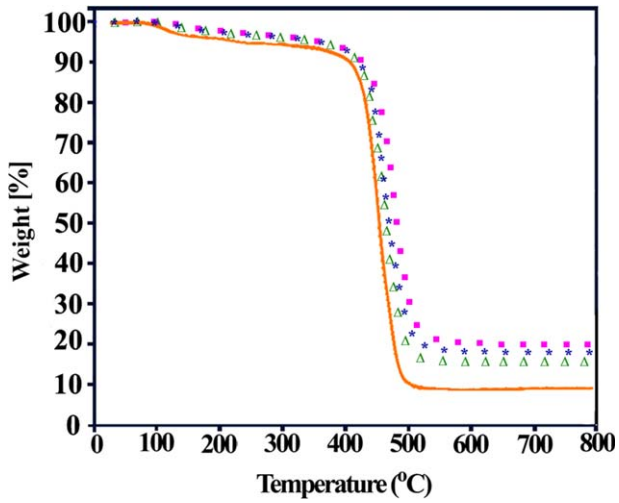

Figure 10. TGA thermograms of PVP, PMFA (3 wt %), PMFA (5 wt %), and PMFA (7 wt %) under nitrogen atmosphere at heating rate of 20 °C/min. [Color figure can be viewed in the online issue, which is available at wileyonlinelibrary.com.]

Table I. Thermal Properties of the Pure PVP and PMFA NCs

Sample	T_5 (°C)[a]	T_{10} (°C)[b]	Char yield (%)[c]	LOI[d]
PVP	227	403	9	21
PMFA NC 3 wt %	339	416	15	23
PMFA NC 5 wt %	345	420	18	25
PMFA NC 7 wt %	348	423	20	26

[a] Temperature at which 5% weight loss was recorded by TGA at heating rate of 20 °C/min under a nitrogen atmosphere.
[b] Temperature at which 10% weight loss was recorded by TGA at heating rate of 20 °C/min under a nitrogen atmosphere.
[c] Weight percentage of material left undecomposed after TGA analysis at a temperature of 800 °C under a nitrogen atmosphere.
[d] Limiting oxygen index (LOI) evaluating char yield at 800 °C.

Thermal Properties

The thermal behavior of the MFA and DM-MFA, PVP, and the obtained NCs were investigated by TGA, as presented in Figures 9 and 10. According to Figure 9, the first weight loss for MFA and DM-MFA corresponded to the removal of moisture and physisorbed water in the range of 100 to 200 °C.[54] MFA demonstrates weight loss about 3.5% within a temperature range of 100 to 200 °C, 2.5% in 200 to 420 °C. While the grafted one shows more weight loss attributed to the decomposition of TML that hydrogen bonded to the surface groups of MFA nanocrystals. Figure 10 displays the TGA curves obtained in nitrogen for pristine PVP[55] and the obtained composites. The TGA curves of the PMFA NCs demonstrate a one-step weight loss. A comparative thermal analysis of the polymer, and the aforesaid NCs reveals an improved thermal stability in case of PMFA NCs over the neat PVP, which could be due to strong interfacial interactions between modified particles and polymer matrix. As can be seen, until 800 °C the total weight loss of the NCs is much lower than that of the pure PVP, signifying that thermal stability of the obtained NCs is developed noticeably. Table I demonstrates the corresponding thermoanalysis data, including the temperatures at which 5% (T_5) and 10% (T_{10}) degradation occurred. The residue at 800 °C (char yield) and similarly limiting oxygen index (LOI) consistent with Van Krevelen and Hoftyzer equation [eq. (2)] were determined from the original thermograms.[56]

$$\mathrm{LOI} = 17.5 + 0.4\ \mathrm{CR} \tag{2}$$

where CR = char yield.

On the other hand, the char yield of the pure PVP at 800 °C is 9%, whilst those of the NCs at 800 °C, are in the range of 15 to 20%. The char yield of the obtained NCs was improved as the content of DM-MFA was increased, owing to the high thermal resistance of ceramic and the physical crosslink points of the MFA particles. The potential reason for this performance may be the reducing degradation process by reason of the reduced mobility of chain transfer reaction. Additionally, the improvement in the char yield of the obtained materials was due to the strong hydrogen bonding between PVP matrix and free acid functionalized groups of DM-MFA.

CONCLUSIONS

The results obtained in the current study can be summarized as follows. The surface modification of nanofillers is a very significant field due to the surface of them plays an important role in the properties of NPs, including the solubility, dispersity, stability, and so on. Thus, at first the surface of MFA particles could be modified with bioactive TML through ultrasonic technique without changing their crystal structure and morphology. The FT-IR analyses demonstrated that TML containing natural amino acid were strongly hydrogen-bonded to the surface groups of MFA. Also, the novel organo-mineral NCs based on PVP and DM-MFA was fabricated by a single-step, fast and easy procedure. The use of TML as a coupling agent provides a substantial platform for better dispersion of DM-MFA in the PVP matrix as has been confirmed from TEM and FE-SEM studies. The thermal stability of the PMFA NCs was also rather improved by increasing the amount of DM-MFA NPs. Since modified MFA with bioactive TML is ecofriendly and biodegradable, they could be used in many applications such as production of bionanocomposites. Similarly, incorporation of modified apatite in organic matrix proposes the probability of the construction of a series of NCs with a high potential for new application.

ACKNOWLEDGMENTS

The authors approvingly acknowledge the financial support of the Research Affairs Division of Isfahan University of Technology (IUT), Isfahan. Additional financial support from National Elite Foundation (NEF) of Iran, and Iran nanotechnology Initiative Council (INIC) also thankfully acknowledged.

REFERENCES

1. Hanemann, T.; Szabo, D. V. *Materials* **2010**, *3*, 3468.
2. Webster, T. J., Ed. Safety of Nanoparticles from Manufacturing to Medical Applications; Springer: New York, **2009**.
3. Kassing, R.; Petkov, P.; Kulisch, W.; Popov, C., Eds. Functional Properties of Nanostructured Materials; Springer: Netherlands, **2006**.
4. Mallakpour, S.; Javadpour, M. *J. Appl. Polym. Sci.* **2016**, *133*. DOI: 10.1002/app.43433.
5. Arjomandi, J.; Keramat Irad Mossa, N.; Jaleh, B. *J. Appl. Polym. Sci.* **2015**, *132*. DOI: 10.1002/app.41526
6. El Miri, N.; Abdelouahdi, K.; Zahouily, M.; Fihri, A.; Barakat, A.; Solhy, A.; El Achaby, M. **2015**, *132*. DOI: 10.1002/app.42004
7. Volkov, V. V.; Klechkovskaya, V. V.; Shtykova, E. V.; Dembo, K. A.; Arkharova, N. A.; Ivakin, G. I.; Smyslov, R. Y. *Crystallogr. Rep.* **2009**, *54*, 169.
8. Yazdi Mamaghani, M.; Pishvaei, M.; Kaffashi, B. *Macromol. Res.* **2011**, *19*, 243.
9. Stipniece, L.; Narkevica, I.; Sokolova, M.; Locs, J.; Ozolins, J. *Ceram. Int.* **2016**, *42*, 1530.
10. Supova, M. *J. Mater. Sci. Mater. Med.* **2009**, *20*, 1201.
11. Onoki, T.; Nakahira, A.; Tago, T.; Hasegawa, Y.; Kuno, T. *Appl. Surf. Sci.* **2012**, *262*, 263.
12. Castelan-Velazco, L. I.; Mendez-Nonell, J.; Sanchez-Valdes, S.; Ramos-deValle, L. F. *Polym. Bull.* **2009**, *62*, 99.
13. Waszkiel, D.; Opalko, K.; Łagocka, R.; Chlubek, D. *Fluoride* **2004**, *37*, 271.
14. Montazeri, N.; Jahandideh, R.; Biazar, E. *Int. J. Nanomed.* **2011**, *6*, 197.
15. Nikcevic, I.; Jokanovic, V.; Mitric, M.; Nedic, Z.; Makovec, D.; Uskokovic, D. *J. Solid State Chem.* **2004**, *177*, 2565.
16. Ebrahimi-Kahrizsangi, R.; Nasiri-Tabrizi, B.; Chami, A. *Solid State Sci.* **2010**, *12*, 1645.
17. Landi, E.; Logroscino, G.; Proietti, L.; Tampieri, A.; Sandri, M.; Sprio, S. *J. Mater. Sci. Mater. Med.* **2008**, *19*, 239.
18. Cai, Y.; Zhang, S.; Zeng, X.; Wang, Y.; Qian, M.; Weng, W. *Thin Solid Films* **2009**, *517*, 5347.
19. Nasiri-Tabrizi, B.; Fahami, A. ISRN Ceram 2012, *9*, 1, DOI: 10.5402/2012/754704.
20. Ahn, E. S.; Gleason, N. J.; Ying, J. Y. *J. Am. Ceram. Soc.* **2005**, *88*, 3374.
21. Pramanik, N.; Mohapatra, S.; Bhargava, P.; Pramanik, P. *Mater. Sci. Eng. C* **2009**, *29*, 228.
22. Asefnejad, A.; Behnamghader, A.; Khorasani, M. T.; Farsadzadeh, B. *Int. J. Nanomed.* **2011**, *6*, 93.
23. Chen, M.; Tan, J.; Lian, Y.; Liu, D. *Appl. Surf. Sci.* **2008**, *254*, 2730.
24. Xu, X.; Chen, X.; Liu, A.; Hong, Z.; Jing, X. *Eur. Polym. J.* **2007**, *43*, 3187.
25. D'Andrea, S. C.; Fadeev, A. Y. *Langmuir* **2003**, *19*, 7904.
26. Aissa, A.; Debbabi, M.; Gruselle, M.; Thouvenot, R.; Gredin, P.; Traksmaa, R.; Tonsuaadu, K. *J. Solid State Chem.* **2007**, *180*, 2273.
27. Lee, H. J.; Choi, H. W.; Kim, K. J.; Lee, S. C. *Chem. Mater.* **2006**, *18*, 5111.
28. Aissa, A.; Agougui, H.; Debbabi, M. *Appl. Surf. Sci.* **2011**, *257*, 9002.
29. Choi, H. W.; Lee, H. J.; Kim, K. J.; Kim, H. M.; Lee, S. C. *J. Colloid Interface Sci.* **2006**, *304*, 277.
30. Jarlbring, M.; Sandstrom, D. E.; Antzutkin, O. N.; Forsling, W. *Langmuir* **2006**, *22*, 4787.
31. Jarlbring, M. Doctoral Thesis, Lulea University of Technology, Sweden, **2006**.
32. Tanaka, H.; Futaoka, M.; Hino, R. *J. Colloid Interface Sci.* **2004**, *269*, 358.
33. Jing, C.; Xu, X.; Zhang, X.; Liu, Z.; Chu, J. *J. Phys. D: Appl. Phys.* **2009**, *42*, 075402.
34. Kobayashi, Y.; Kosuge, A.; Konno, M. *Appl. Surf. Sci.* **2008**, *255*, 2723.
35. Wang, B. L.; Liu, X. S.; Ji, Y.; Ren, K. F.; Ji, J. *Carbohydr. Polym.* **2012**, *90*, 8.
36. Mendes, L. C.; Rodrigues, R. C.; Silva, E. P. *J. Therm. Anal. Calorim.* **2010**, *101*, 899.
37. Topkaya, R.; Kurtan, U.; Baykal, A.; Toprak, M. S. *Ceram. Int.* **2013**, *39*, 5651.
38. Zakeri, M.; Shademan, M. *Arab. J. Sci. Eng.* **2014**, *39*, 2227.

39. Mostafa, A. A.; Oudadesse, H.; Mohamed, M. B.; Foad, E. S.; Le Gal, Y.; Cathelineau, G. *Chem. Eng. J.* **2009**, *153*, 187.
40. Suchanek, W. L.; Byrappa, K.; Shuk, P.; Riman, R. E.; Janas, V. F.; TenHuisen, K. S. *Biomaterials* **2004**, *25*, 4647.
41. Kumar, A.; Choudhary, V.; Negi, Y. S.; Bhardwaj, N. K. *Cellulose* **2014**, *21*, 3409.
42. Mohammadi Zahrani, E.; Fathi, M. H.; Alfantazi, A. M. *Metall. Mater. Trans. A* **2011**, *42*, 3291.
43. Fereshteh, Z.; Mallakpour, F.; Fathi, M. H.; Mallakpour, S.; Bagri, A. *Ceram. Int.* **2015**, *41*, 10079.
44. Staubli, A.; Ron, E.; Langer, R. *J. Am. Chem. Soc.* **1990**, *112*, 4419.
45. Mallakpour, S.; Banihassan, K.; Sabzalian, M. R. *J. Polym. Environ.* **2013**, *21*, 568.
46. Kheradmandfard, M.; Fathi, M. H. *Ceram. Int.* **2013**, *39*, 1651.
47. Rapacz-Kmita, A.; Paluszkiewicz, C.; Slosarczyk, A.; Paszkiewicz, Z. *J. Mol. Struct.* **2005**, *744*, 653.
48. Liu, Y.; Wang, W.; Zhan, Y.; Zheng, C.; Wang, G. *Mater. Lett.* **2002**, *56*, 496.
49. Murugan, R.; Ramakrishna, S. *J. Cryst. Growth* **2005**, *274*, 209.
50. Williamson, G. K.; Hall, W. H. *Acta Metall.* **1953**, *1*, 22.
51. Abd El-kader, M. F. H.; Abu-Abdeen, M. *Aust. J. Basic Appl. Sci.* **2012**, *6*, 454.
52. Vouvoudi, E.; Panytsidou, T.; Sotiropoulos, S.; Pavlidou, E.; Sideridou, I. *Polym. Plast. Technol. Eng.* **2015**, *54*, 1596.
53. Khulbe, K. C.; Kruczek, B.; Chowdhury, G.; Gagne, S.; Matsuura, T. *J. Appl. Polym. Sci.* **1996**, *59*, 1151.
54. Hidouri, M.; Bouzouita, K.; Kooli, F.; Khattech, I. *Mater. Chem. Phys.* **2003**, *80*, 496.
55. Mallakpour, S.; Khani, M. *Polym. Bull.* **2016**, 1.
56. Van Krevelen, D. W.; Hoftyzer, P. J. Properties of Polymers, 3rd ed.; Elsevier: Amsterdam, **1976**.